The Hertz contact problem in couple-stress elasticity

P.A. Gourgiotis, Th. Zisis, A.E. Giannakopoulos, H.G. Georgiadis

PII: S0020-7683(19)30156-8
DOI: https://doi.org/10.1016/j.ijsolstr.2019.03.032
Reference: SAS 10325

To appear in: *International Journal of Solids and Structures*

Received date: 3 January 2019
Revised date: 21 March 2019
Accepted date: 27 March 2019

Please cite this article as: P.A. Gourgiotis, Th. Zisis, A.E. Giannakopoulos, H.G. Georgiadis, The Hertz contact problem in couple-stress elasticity, *International Journal of Solids and Structures* (2019), doi: https://doi.org/10.1016/j.ijsolstr.2019.03.032

The Hertz contact problem in couple-stress elasticity

P.A. Gourgiotis[1], Th. Zisis[2,*], A.E. Giannakopoulos[2], H.G. Georgiadis[2,3]

[1] Department of Engineering, Durham University,
South Road, Durham, DH1 3LE, UK
[2] Mechanics Division, National Technical University of Athens,
Zographou, GR-15773, Greece
[3] Office of Theoretical and Applied Mechanics,
Academy of Athens, Greece

March 29, 2019

Abstract

The classical three-dimensional Hertz contact problem is re-examined in the present work within the context of couple-stress elasticity. This theory introduces characteristic material length scales that emerge from the underlying microstructure and has proved to be very effective yet rather simple for modeling complex microstructured materials. An exact solution of the axisymmetric contact problem is obtained through Hankel integral transforms and singular integral equations. The goal is to examine to what extend this gradient theory captures the experimentally observed indentation response and the related size effects in materials with microstructure. Furthermore, the present work extends the classical Hertz contact solution in the framework of a generalized continuum theory providing thus a useful theoretical background for the interpretation of spherical indentation tests of microstructured materials. The results obtained in the present work can be used in order to model nano/micro indentation experiments of several materials, such as polymers, ceramics, composites, cellular materials, foams, masonry, and bone tissues, of which their macroscopic response is influenced by the microstructural characteristic lengths.

Keywords: size-effects, polymers; microstructure; Cosserat elasticity; spherical indentation

*Corresponding author: Th. Zisis. Email: zisis@mail.ntua.gr

1 Introduction

The celebrated Hertz 3D contact problem is revisited in this work in the context of couple-stress elasticity. The Hertz problem involves a half-space whose surface is indented by a rigid spherical indenter. The original solution was first published in 1882 by Heinrich Hertz in his seminal paper "On the contact of elastic solids" (Hertz, 1882). Hertz worked towards the understanding of the effect of the force applied on multiple stacked lenses upon their optical properties. Hertz showed that the contact stress that develops as two curved surfaces come in contact and deform under the imposed loads depends upon the normal contact force, the radii of curvature of both bodies as well as the modulus of elasticity of both bodies. The Hertzian contact solution is the building block of elastic contact mechanics with a wide range of applicability ranging from geotechnical applications where the solution is used determine the load bearing capacity of soil to the determination of the fatigue life in bearings, gears, and any other bodies where two surfaces are in contact.

The Hertz contact solution has been extensively used as the basis for the spherical indentation testing technique which is commonly applied for the determination of material properties and the characterization of deformation behaviour at small length scales. As the contact scales in such experiments reduce progressively (from micro to nano-scales) the internal material lengths become important and their effect upon the macroscopic response cannot be ignored. There is ample experimental evidence from different indentation experiments in metals (Cao et al., 2006) and polymers (Briscoe et al., 1998; Chong et al., 1999; Dutta et al., 2004; Zhang et al., 2002; Shen et al., 2005) that the produced deformation is length scale dependent. While in metals this length scale dependent deformation is associated with geometrically necessary dislocations (Nix and Gao, 1998), in polymers size effects have been associated with elastic deformations (McFarland and Colton, 2005; Alisafaei et al., 2014). In particular, size effects in polymers have been attributed to surface effects (Zhang and Xu, 2002; Zhang et al., 2004),

friction (Lim and Chaudhri, 2006), tip imperfections (Flores and Calleja, 1998), material inhomogeneities (Briscoe et al., 1998), surface adhesion (Johnson et al., 1971), as well as multi-physics phenomena such as piezoelectricity (Giannakopoulos amd Suresh, 1999), magnetoelasticity (Giannakopoulos end Parmaklis, 2007), and flexoelectricity (Mao et al., 2016). It seems, however, that the contact related size phenomenon is mainly the result of the imposed higher order displacement gradients emerging in the vicinity of the tip of the indentor (Briscoe et al., 1998; Chong and Lam, 1999; Alisafaei et al., 2014; Lam and Chong, 1999; Lam and Chong, 2000; Lam and Chong, 2001; Swaddiwudhipong et al., 2005; Nikolov et al., 2007; Han, 2010; Alisafaei et al., 2013; Voyiadjis et al., 2014; Garg et al., 2016). It has been further shown that size effects in elastomers are considerably more pronounced than in thermoset or thermoplastic polymers in which the size effect is attributed to their molecular structure.

In the present study, we examine the static spherical indentation technique in the context of the couple stress elasticity theory. The couple-stress theory is the simplest gradient type generalized continuum theory where higher order deformation gradients arise and it has been proven very effective in modelling microstructured materials. In particular, the couple-stress theory assumes an augmented form of the Euler-Cauchy principle with a non-vanishing couple traction, and a strain-energy density that depends upon both the strain and the gradient of rotation. An isotropic couple-stress material is described by four material parameters in the three-dimensional case. Two of them have an analogous meaning with the Lame constants of classical theory and the additional two are related to the bending and the torsional stiffness at the material point. The additional parameters can be expressed in terms of a characteristic length, the existence of which shows that the couple-stress theory encompasses the possibility of analytically describing size effects.

The present study extends the classical Hertz contact solution in the framework of a generalized continuum theory. It is expected that this work may essentially

provide a useful theoretical basis for the interpretation of spherical indentation tests of microstructured materials and the related size effects. The results obtained can be used to model nano/micro indentation experiments of several materials of which their macroscopic response is strongly influenced by the microstructural characteristic lengths, such as polymers, ceramics, composites, cellular materials, foams, masonry, and bone tissues.

2 Fundamentals of couple-stress elasticity

In the theory of couple–stress elasticity, also known as Cosserat theory with constrained rotations, the modified strain–energy density and the resulting constitutive relations involve, besides the usual infinitesimal strains, certain strain gradients known as the rotation gradients (Mindlin and Tiersten, 1962; Koiter, 1964). The generalized stress–strain relations for the isotropic case include, in addition to the conventional pair of elastic constants, two new elastic constants, one of which is expressible in terms of a material parameter that has dimensions of length. The presence of this length parameter, in turn, implies that the modified theory encompasses the possibility of size effects. In fact, the couple-stress elasticity theory has been already employed successfully to model size effects in fracture (Gourgiotis and Georgiadis, 2007; Radi, 2008; Mishuris et al., 2012; Morini et al., 2013) and contact problems (Zisis et al., 2014; Zisis, 2017; Karuriya and Bhandakkar, 2017; Song et al., 2017). It should be further noted that only few three dimensional solutions exist within the context of gradient theories with the majority of them concerning traction boundary value problems for concentrated or distributed loads (see for example Ejike, 1970; Anagnostou et al., 2013; Gao and Zhou, 2013; Georgiadis et al., 2014);

We begin by giving a brief account of the theory of couple–stress elasticity. A thorough account of the anisotropic couple-stress theory is given in (Gourgiotis and Bigoni, 2016; Bigoni and Gourgiotis, 2016) In the absence of inertia effects

and body loads, the balance laws for the linear and angular momentum lead to the following force and moment equations of equilibrium (Mindlin and Tiersten, 1962)

$$\sigma_{ji,j} = 0, \qquad e_{ijk}\sigma_{jk} + m_{ji,j} = 0, \tag{1}$$

where a Cartesian rectangular coordinate system $Oxyz$ is used along with indicial notation and summation convention. In these equations σ_{ij} is the force–stress tensor, m_{ij} is the couple-stress tensor, comma denotes partial differentiation and e_{ijk} is Levi–Civita alternating symbol. Further, σ_{ij} can be decomposed into its symmetric and anti-symmetric components as follows

$$\sigma_{ij} = \tau_{ij} + \alpha_{ij}, \tag{2}$$

with $\tau_{ij} = \tau_{ji}$ and $\alpha_{ij} = -\alpha_{ji}$. Using (2), the anti-symmetric part of the stress tensor can be written as

$$\alpha_{ij} = -\frac{1}{2} e_{ijk} m_{pk,p} \tag{3}$$

from which follows that the stress tensor is symmetric for a vanishing divergence of couple-stresses.

Concerning the kinematical description of the continuum, the following primary kinematical fields are defined in the framework of the geometrically linear theory

$$\varepsilon_{ij} = \frac{1}{2}\left(u_{j,i} + u_{i,j}\right), \quad \omega_i = \frac{1}{2} e_{ijk} u_{k,j}, \quad \kappa_{ij} = \omega_{j,i}. \tag{4}$$

where ε_{ij} is the strain tensor, ω_i is the rotation vector, and κ_{ij} is the curvature tensor (i.e. the gradient of rotation or the curl of the strain) expressed in dimensions of [length]$^{-1}$, which by definition is traceless: $\kappa_{ii} = 0$ since $\omega_{i,i} = 0$.

Regarding the boundary conditions, we note that in the constrained couple-stress theory the normal component of the rotation vector is fully specified by the distribution of tangential displacements over the boundary. This implies that the traction boundary conditions, at any point on a smooth boundary or section,

consist of the following three reduced force-tractions and two tangential couple-tractions

$$P_i^{(n)} = \sigma_{ji} n_j - \frac{1}{2} e_{ijk} n_j m_{(nn),k}, \quad R_i^{(n)} = m_{ji} n_j - m_{(nn)} n_i \tag{5}$$

where $m_{(nn)} = n_i n_j m_{ij}$ is the normal component of the couple-stress tensor m_{ij}, and n_i are the components of the unit vector outward normal to the surface.

Assuming a linear and isotropic material response, the constitutive equations for an isotropic couple-stress medium become

$$\tau_{ij} = \lambda \varepsilon_{kk} \delta_{ij} + 2\mu \varepsilon_{ij}, \quad m_{ij} = 4\eta \kappa_{ij} + 4\eta' \kappa_{ji} \tag{6}$$

where the moduli (λ, μ) have the same meaning as the Lamè constants of classical elasticity theory and are expressed in dimensions of [force][length]$^{-2}$, and the moduli (η, η') account for couple–stress effects and are expressed in dimensions of [force].

Incorporating now the constitutive relations (6) into the equations of equilibrium (1), and using the geometric relations (4), one may obtain the equations of equilibrium in terms of the displacements

$$\nabla^2 \mathbf{u} + (\lambda + \mu) \nabla (\nabla \cdot \mathbf{u}) - \mu \ell^2 \nabla^2 \left[\nabla^2 \mathbf{u} - \nabla (\nabla \cdot \mathbf{u}) \right] = 0 \tag{7}$$

where $\ell \equiv (\eta / \mu)^{1/2}$ is the characteristic material length. In the limit $\ell \to 0$, the Navier-Cauchy equations of classical linear isotropic elasticity are recovered from (9). Mindlin and Tiersten (1962) have shown that the displacement vector $\mathbf{u}$ in (9) can be expressed as:

$$\mathbf{u} = \mathbf{B} - \ell^2 \nabla \nabla \cdot \mathbf{B} - \frac{\lambda + \mu}{2(\lambda + 2\mu)} \nabla \left(\mathbf{x} \cdot \left(1 - \ell^2 \nabla^2 \right) \mathbf{B} + B_0 \right), \tag{8}$$

where $\mathbf{x}$ is the position vector, $\mathbf{B}$ is a vector function satisfying

$$\left(1-\ell^2\nabla^2\right)\nabla^2\mathbf{B}=\mathbf{0}, \tag{9}$$

and B_0 a scalar function such that:

$$\nabla^2 B_0 = 0. \tag{10}$$

Since we are aiming towards a solution of the axisymmetric Hertz contact problem, a cylindrical coordinate system (r,θ,z) will be employed. Through simple coordinate transformations, we find that the non-vanishing components of the rotation vector and the curvature-twist tensor, Eq. (4), are given in the axisymmetric case by (Ejike, 1969)

$$\omega_\theta=\frac{1}{2}\left(\frac{\partial u_r}{\partial z}-\frac{\partial u_z}{\partial r}\right),\quad \kappa_{\theta r}=-\frac{\omega_\theta}{r},\quad \kappa_{r\theta}=\frac{\partial \omega_\theta}{\partial r}\quad \kappa_{z\theta}=\frac{\partial \omega_\theta}{\partial z}, \tag{11}$$

where $u_r(r,z)$ and $u_z(r,z)$ are the components of the displacement vector in cylindrical coordinates. Note that all quantities are independent of the angular coordinate θ and that $u_\theta=0$.

The non-vanishing components of the couple-stress tensor become then

$$\begin{aligned} &m_{r\theta}=4\mu\ell^2\left(\frac{\partial\omega_\theta}{\partial r}-\frac{\beta}{r}\omega_\theta\right),\quad m_{\theta r}=4\mu\ell^2\left(\beta\frac{\partial\omega_\theta}{\partial r}-\frac{1}{r}\omega_\theta\right),\\ &m_{z\theta}=4\mu\ell^2\frac{\partial\omega_\theta}{\partial z},\quad m_{\theta z}=4\mu\beta\ell^2\frac{\partial\omega_\theta}{\partial z}=\beta m_{z\theta}, \end{aligned} \tag{12}$$

where $\beta=\eta'/\eta$ is a dimensionless parameter that varies in the range: $-1<\beta<1$. Accordingly, using (3), the only non vanishing component of the antisymmetric part of the stress tensor reads

$$\alpha_{zr}=-\alpha_{rz}=-\frac{1}{2}\left(\frac{\partial m_{r\theta}}{\partial r}+\frac{m_{r\theta}+m_{\theta r}}{r}+\frac{\partial m_{z\theta}}{\partial z}\right). \tag{13}$$

Further, for a flat boundary that is characterized by the unit normal $\mathbf{n}=$

$(0, 0, 1)$, the reduced force-stress tractions defined by (5) read in cylindrical coordinates:

$$P_r^{(n)} = \sigma_{zr} = \tau_{zr} + \alpha_{zr} = \\ = \mu \left[\frac{\partial u_r}{\partial z} + \frac{\partial u_z}{\partial r} - \ell^2 \left(\frac{\partial^2}{\partial r^2} + \frac{1}{r}\frac{\partial}{\partial r} - \frac{1}{r^2} + \frac{\partial^2}{\partial z^2} \right) \left(\frac{\partial u_r}{\partial z} - \frac{\partial u_z}{\partial r} \right) \right], \tag{14}$$

Note that $m_{(nn)} = m_{zz} = 0$ in the axisymmetric case considered here.

$$P_z^{(n)} = \sigma_{zz} = \lambda \frac{1}{r}\frac{\partial}{\partial r}\left(r\, u_r\right) + (\lambda + 2\mu)\frac{\partial u_z}{\partial z}, \qquad P_\theta^{(n)} \equiv 0, \tag{15}$$

while, the couple-stress tractions become

$$R_\theta^{(n)} = m_{z\theta} = 2\mu\ell^2 \frac{\partial}{\partial z}\left(\frac{\partial u_r}{\partial z} - \frac{\partial u_z}{\partial r} \right), \tag{16}$$

$$R_r^{(n)} \equiv R_z^{(n)} \equiv 0. \tag{17}$$

Taking $\mathbf{B}$ to be the vector $(0,\ 0,\ \Psi)$ and B_0 the scalar function Φ, where Φ and Ψ are functions of (r, z), Eqs (8) give

$$u_r = -\frac{\partial}{\partial r}\left[\ell^2 \frac{\partial \Psi}{\partial z} + \alpha \left(z \left(1 - \ell^2 \nabla^2 \right) \Psi + \Phi \right) \right], \tag{18}$$

$$u_z = \Psi - \ell^2 \frac{\partial^2 \Psi}{\partial z^2} - \alpha \frac{\partial}{\partial z}\left(z \left(1 - \ell^2 \nabla^2 \right) \Psi + \Phi \right), \tag{19}$$

$$\omega_\theta = -\frac{1}{2}\frac{\partial \Psi}{\partial r}, \tag{20}$$

where

$$\alpha = \frac{\lambda + \mu}{2\left(\lambda + 2\mu\right)} = \frac{1}{4\left(1 - \nu\right)} \tag{21}$$

with ν being the Poisson's ratio. The functions (Φ, Ψ) satisfy the differential

equations

$$\nabla^2\Phi = 0, \qquad \left(1-\ell^2\nabla^2\right)\nabla^2\Psi = 0, \tag{22}$$

with

$$\nabla^2 = \frac{\partial^2}{\partial r^2} + \frac{1}{r}\frac{\partial}{\partial r} + \frac{\partial^2}{\partial z^2}. \tag{23}$$

As a final comment, before proceeding any further, we note that the governing equations (22) and the tractions defined on flat boundary do not depend upon the dimensionless parameter β for the case of the axisymmetric deformation.

3 Formulation of the contact problem and Hankel transform analysis

Consider a traction-free elastic half-space defined by $z \geq 0$, whose surface is intended by a rigid spherical indenter of radius R as shown in Fig. 1. The indenter is pressed in contact with the half-space under the action of a force P. The vertical displacement of the points on the surface ($z = 0$) within the contact area is given as

$$w(r) \equiv u_z(r,0) = \delta - \frac{r^2}{2R}, \quad \text{for} \quad 0 < r < a, \tag{24}$$

where a is the contact radius and δ is the maximum penetration depth of the indenter, i.e. $\delta = u_z\,(r=0,\ z=0)$. Note that the quantity δ will be specified through the solution of the problem. For a frictionless and smooth contact, the traction boundary conditions within the context of couple-stress elasticity may then be written as (Shu and Fleck, 1998)

$$\sigma_{zz}(r,0) = 0, \quad \text{for} \quad a < r < \infty, \tag{25}$$

$$\sigma_{zr}(r,0) = 0, \quad \text{for} \quad 0 < r < \infty, \tag{26}$$

$$m_{z\theta}(r,0) = 0, \quad \text{for} \quad 0 < r < \infty, \tag{27}$$

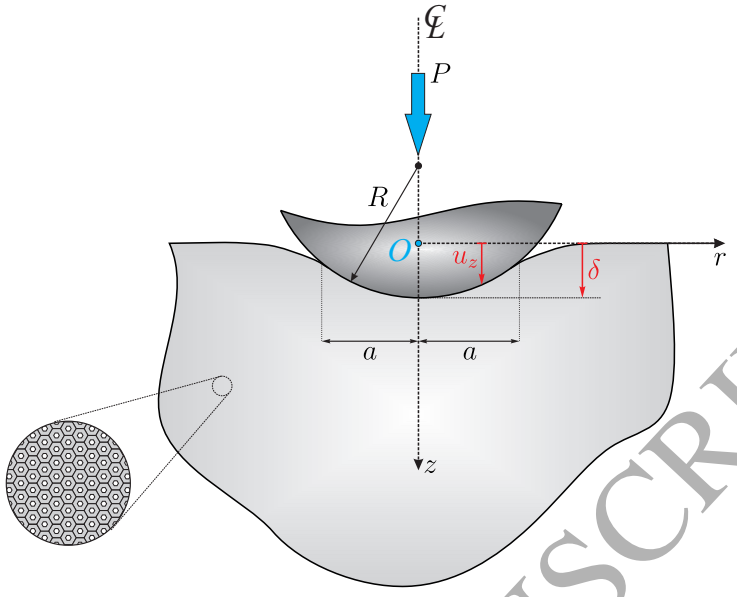

Figure 1: Spherical indentation by a rigid indenter of an elastic traction free half-space with an indicative microstructure. The shear modulus of the half-space is μ, the Poisson's ratio is ν and the internal microstructural length scale is ℓ.

within the contact region the normal traction becomes equal to the pressure $p\,(r)$ below the indentor:

$$\sigma_{zz}(r,0) = -p(r) \quad \text{for} \quad 0 \leq r < a. \tag{28}$$

The axisymmetric nature of the Hertz contact problem lends itself to a Hankel transform analysis. The direct and inverse Hankel transforms of the n^{th}-order of a function $f(r,z)$ with respect to r are defined, respectively, as

$$\mathcal{H}_n\left[f(r,z)\right] = \int_0^\infty r\, f\,(r,z)\, J_n\,(\xi r)\; dr, \tag{29}$$

$$\mathcal{H}_n^{-1}\left[\hat{f}(\xi,z)\right] = \int_0^\infty \xi\, \hat{f}\,(\xi,z)\, J_n\,(\xi r)\; d\xi, \tag{30}$$

where J_n is the Bessel function of the first kind.

Applying the Hankel transform to the governing field equations (22), we obtain

the following representations for the functions Φ and Ψ suitable for $z \geq 0$:

$$\Phi(r,z) = \mathcal{H}_0^{-1}\left[\xi^{-1} A(\xi)\, e^{-\xi z}\right], \tag{31}$$

$$\Psi(r,z) = \mathcal{H}_0^{-1}\left[\xi^{-1}\left\{B(\xi)\, e^{-\xi z} + C(\xi)\, e^{-\zeta z/\ell}\right\}\right], \tag{32}$$

where $\zeta = (1+\ell^2\xi^2)^{1/2}$.

The functions $A(\xi)$, $B(\xi)$, and $C(\xi)$ are determined using the traction boundary conditions in (25). In particular, we obtain

$$A \equiv A(\xi) = \frac{2(1-\nu)}{\mu\xi N(\xi)}\left[N(\xi) - 2(1-\nu)\,\zeta\right]\hat{p}(\xi), \tag{33}$$

$$B \equiv B(\xi) = \frac{2(1-\nu)\,\zeta}{\mu N(\xi)}\hat{p}(\xi), \quad C \equiv C(\xi) = -\frac{2\ell(1-\nu)\,\xi}{\mu N(\xi)}\hat{p}(\xi), \tag{34}$$

with

$$N(\xi) = \zeta + 4(1-\nu)\,\ell^2\xi^2(\zeta - \ell\xi), \tag{35}$$

and $\hat{p}(\xi)$ is the transformed pressure below the indentor defined as

$$\hat{p}(\xi) = \int_0^\infty r\, p(r)\, J_0(\xi r)\, dr = \int_0^a r\, p(r)\, J_0(\xi r)\, dr \tag{36}$$

where use of (28) has been made.

Utilizing the kinematic relations in (18) in conjunction with the constitutive equations (6), we express the displacement rotation and the relevant stress components, at any point of the half-space $z \geq 0$, as

$$u_r(r,z) = \mathcal{H}_1^{-1}\left[\xi^{-1}\left\{\left[\alpha(1+\xi z) - \frac{1}{2}\right] e^{-\xi z}\, B + \gamma(\xi,z)\, C\right\}\right], \tag{37}$$

$$u_z(r,z) = \mathcal{H}_0^{-1}\left[\xi^{-1}\left\{\left(\frac{1}{2}+\alpha\,\xi\,z\right)\,e^{-\xi z}B + \ell^2\,\xi^2\left(e^{-\xi\,z}-e^{-\zeta z/\ell}\right)C\right\}\right], \tag{38}$$

$$\omega_\theta(r,z) = \mathcal{H}_1^{-1}\left[\frac{1}{2}\left(e^{-\xi\,z}B + e^{-\zeta z/\ell}C\right)\right], \tag{39}$$

$$\sigma_{zz}(r,z) = -2\mu\mathcal{H}_0^{-1}\left[\alpha\,(1+\xi\,z)\,e^{-\xi\,z}B + \gamma(\xi,z)\,C\right], \tag{40}$$

$$\begin{aligned}\sigma_{rr}(r,z) = {} & 2\mu\mathcal{H}_0^{-1}\left[(1+\alpha\,(\xi z-3))\;e^{-\xi\,z}\,B+\gamma(\xi,z)\,C\right]\\ & -\frac{2\mu}{r}\mathcal{H}_1^{-1}\left[\xi^{-1}\left\{\left(\frac{1}{2}+\alpha\,(\xi z-1)\right)e^{-\xi\,z}\,B+\gamma(\xi,z)\,C\right\}\right],\end{aligned} \tag{41}$$

$$\begin{aligned}\sigma_{\theta\theta}(r,z) = {} & (1-4\alpha)\,\mu\mathcal{H}_0^{-1}\left[e^{-\xi z}\,B\right]\\ & +\frac{2\mu}{r}\mathcal{H}_1^{-1}\left[\xi^{-1}\left\{\left[\frac{1}{2}+\alpha\,(\xi z+1)\right]e^{-\xi\,z}\,B+\gamma(\xi,z)\,C\right\}\right],\end{aligned} \tag{42}$$

with $\gamma(\xi,z) = \ell\,\xi\left(\ell\,\xi\,e^{-\xi\,z} - \zeta e^{-\zeta z/\ell}\right)$.

The surface vertical displacement becomes then

$$w\,(r) = \frac{(1-\nu)}{\mu}\int_0^\infty G\,(\xi)\,\hat{p}\,(\xi)\,J_0\,(\xi r)\;d\xi \tag{43}$$

with

$$G\,(\xi) = \frac{\sqrt{1+\ell^2\xi^2}}{\sqrt{1+\ell^2\xi^2}+4\,(1-\nu)\,\ell^2\,\xi^2\left(\sqrt{1+\ell^2\xi^2}-\ell\,\xi\right)}. \tag{44}$$

4 Singular integral equation approach

Our objective now is the determination of the contact stress distribution $p\,(r)$ under the indentor and the determination of the contact radius a. For the solution of the mixed boundary value problem, we will employ the method of singular

integral equations. An application of the technique within the context of couple stress elasticity for plane strain crack and contact problems can be found in the works (Gourgiotis and Georgiadis, 2007; Gourgiotis and Georgiadis, 2007) and (Zisis et al., 2014; Gourgiotis et al., 2016; Zisis et al., 2015), respectively.

Combining Eq (43) with (36) and (38), and interchanging the order of integration the vertical surface displacement can be written as

$$w\left(r\right)=\frac{\left(1-\nu\right)}{\mu}\int_{0}^{a}\rho\,\mathbb{K}\left(r,\rho\right)\,p\left(\rho\right)\,d\rho, \tag{45}$$

where the kernel $\mathbb{K}(r,\rho)$ is defined as

$$\mathbb{K}(r,\rho)=\int_{0}^{\infty}G\left(\xi\right)J_{0}\left(\xi\,\rho\right)J_{0}\left(\xi\,r\right)\,d\xi. \tag{46}$$

In order to make the kernel in (45) explicit, we separate its singular and regular parts by examining the asymptotic behaviour of the function $G(\xi)$ as $\xi\to\infty$ by using theorems of the Abel-Tauber type. Noting that

$$G_{\infty}=\lim_{\xi\to\infty}G(\xi)=(3-2\nu)^{-1}, \tag{47}$$

we decompose $G(\xi)$ as follows:

$$G(\xi)=G_{\infty}+\left[G\left(\xi\right)-G_{\infty}\right] \tag{48}$$

and, accordingly, the kernel $\mathbb{K}$ becomes

$$\mathbb{K}(r,\rho)=\frac{1}{3-2\nu}Q_{a}(r,\rho)+Q_{b}(r,\rho) \tag{49}$$

where

$$Q_{a}(r,\rho)=\int_{0}^{\infty}J_{0}(\xi\rho)\,J_{0}(\xi r)\,d\xi=\begin{cases}\dfrac{2}{\pi r}\,\mathrm{K}\left[\dfrac{\rho}{r}\right], & \rho<r\\[2ex] \dfrac{2}{\pi\rho}\,\mathrm{K}\left[\dfrac{r}{\rho}\right], & \rho>r\end{cases}, \tag{50}$$

$$Q_b(r,\rho) = \int_0^\infty \left[G\left(\xi\right) - G_\infty\right]\, J_0(\xi,\rho)\, J_0(\xi r)\, d\xi, \tag{51}$$

with K[ ] being the first kind complete elliptic integral.

The surface displacement takes then the following form

$$w(r) = \frac{(1-\nu)}{\mu(3-2\nu)} \int_0^a \rho\, Q_a(r,\rho)\, p(\rho)\, d\rho + \frac{(1-\nu)}{\mu} \int_0^a \rho\, Q_b(r,\rho)\, p(\rho)\, d\rho, \tag{52}$$

Differentiation of the surface displacement with respect to r yields

$$\frac{\partial w}{\partial r} = \frac{(1-\nu)}{\mu(3-2\nu)} \int_0^a \rho\, \frac{\partial Q_a(r,\rho)}{\partial r}\, p(\rho)\, d\rho + \frac{(1-\nu)}{\mu} \int_0^a \rho\, Q_b'(r,\rho)\, p(\rho)\, d\rho, \tag{53}$$

where

$$Q_b'(r,\rho) = -\int_0^\infty \xi\, [G(\xi) - G_\infty]\, J_1(\xi r)\, J_0(\xi\rho)\, d\xi, \tag{54}$$

$$\frac{\partial Q_a(r,\rho)}{\partial r} = \begin{cases} \dfrac{2}{\pi(\rho^2 - r^2)}\, \mathrm{E}\left[\dfrac{\rho}{r}\right], & \rho < r, \\ \dfrac{2}{\pi\rho\, r}\left(\dfrac{\rho^2}{\rho^2 - r^2}\, \mathrm{E}\left[\dfrac{r}{\rho}\right] - \mathrm{K}\left[\dfrac{r}{\rho}\right]\right), & \rho > r, \end{cases} \tag{55}$$

with E[ ] being the second kind complete elliptic integral.

Following Erdogan (1965) and Civelek and Erdogan (1974), Eq. (53) can be re-written in more convenient form as

$$\frac{\partial w}{\partial r} = \frac{2(1-\nu)}{\mu\pi(3-2\nu)} \int_0^a \frac{r\, h(r,\rho)}{\rho^2 - r^2}\, p(\rho)\, d\rho + \frac{(1-\nu)}{\mu} \int_0^a \rho\, Q_b'(r,\rho)\, p(\rho)\, d\rho, \tag{56}$$

where the function $h(r,\rho)$ is defined as

$$h(r,\rho) = \begin{cases} \dfrac{|\rho|}{|r|}\, \mathrm{E}\left[\dfrac{\rho}{r}\right], & |\rho| < |r|, \\ \dfrac{\rho^2}{r^2}\, \mathrm{E}\left[\dfrac{r}{\rho}\right] - \dfrac{\rho^2 - r^2}{r^2}\, \mathrm{K}\left[\dfrac{r}{\rho}\right], & |\rho| > |r|, \end{cases} \tag{57}$$

with the property $h(r,r) = 1$.

Further, exploiting the fact that $h(r,\rho)$ and $\rho\, Q_b'(r,\rho)$ are even functions with

respect to r and ρ, we extend the definition of the pressure distribution $p(r)$ in (56) to $(-a, a)$. After some algebra, Eq. (56) assumes then the form

$$\begin{aligned}\frac{\partial w}{\partial r} =&\frac{(1-\nu)}{\mu\pi\,(3-2\nu)}\int_{-a}^{a}\frac{p(\rho)}{\rho-r}\,d\rho+\frac{(1-\nu)}{\mu\pi\,(3-2\nu)}\int_{-a}^{a}\Lambda\,(r,\rho)\;p(\rho)\,d\rho\\&+\frac{(1-\nu)}{2\mu}\int_{-a}^{a}|\rho|\,p\,(\rho)\;Q_b'\,(r,\rho)\,d\rho,\end{aligned}\tag{58}$$

where $\Lambda(r,\rho)=\dfrac{h(\rho,r)-1}{\rho-r}$. The function $\Lambda(r,\rho)$ exhibits a logarithmic singularity as $|\rho-r|\to 0$, namely

$$\Lambda(r,\rho)=\frac{1}{2r}\log|\rho-r|+O\,(1)\tag{59}$$

In light of the above and taking into account Eq. (24), the singular integral equation governing the axisymmetric Hertz problem in couple-stress elasticity becomes

$$\begin{aligned}-\frac{(1-\nu)}{\mu\pi\,(3-2\nu)}\int_{-a}^{a}\frac{p\,(\rho)}{r-\rho}\,d\rho+\frac{(1-\nu)}{\mu\pi\,(3-2\nu)}\int_{-a}^{a}\frac{\log|\rho-r|}{2r}\,p\,(\rho)\;d\rho\\+\frac{(1-\nu)}{\mu}\int_{-a}^{a}\mathcal{R}\,(r,\rho)\,p\,(\rho)\;d\rho=-\frac{r}{R},\qquad|r|<R,\end{aligned}\tag{60}$$

where the regular kernel $\mathcal{R}(\rho,r)$ is defined as

$$\mathcal{R}\,(r,\rho)=\frac{|\rho|}{2}\,Q_b'\,(r,\rho)+\frac{1}{\pi\,(3-2\nu)}\left(\Lambda\,(r,\rho)-\frac{\log|\rho-r|}{2r}\right)\tag{61}$$

Furthermore, the equilibrium condition reads

$$P=\pi\int_{-a}^{a}|\rho|\;p(\rho)\,d\rho.\tag{62}$$

As in the classical elasticity theory, the Cauchy singular integral in Eq. (60) dominates the logarithmic kernel and the regular kernel $R(x-t)$ and therefore determines the asymptotic nature of the pressure $p(\rho)$ at the end points of the contact region ($r=a$). In classical elasticity the pressure distribution $p(\rho)$ in the

axisymmetric Hertz contact problem is bounded at the end-points of the contact area (Johnson, 1987). Accordingly, guided also by the results concerning the modification of stress singularities in the presence of couple stresses (Zisis et al., 2014; Gourgiotis et al., 2016; Zisis et al., 2015), one may obtain that the pressure distribution exhibits the following asymptotic behavior: $p(r) = O\left(\sqrt{a^2 - r^2}\right)$ in the vicinity of the contact area. The numerical solution of the singular integral equation (60) together with complementary condition (62) is then obtained using the Gauss-Chebyshev quadrature taking also into account the logarithmic kernel. The general numerical procedure is described in detail in the book of Hills et al. (1996) and in the context of couple stress elasticity in Gourgiotis and Georgiadis (2008) and in Zisis et al. (2014). Once the pressure distribution is known the displacement, rotation, and stresses are found using Eqs (37)-(42).

5 Results and discussion

We now proceed to the discussion of the results obtained for the spherical contact problem. The results are presented in terms of the microstructural ratios: ℓ/a or ℓ/R, and the Poisson's ratio ν.

In Figure 2, we present the effect of the ratio ℓ/a, for constant applied force P, upon the normalized (a) contact radius a/a_c (b) maximum pressure p_0/p_{0c} at the centre of the contact area, and (c) indentation depth δ/δ_c. All couple stress elasticity results have been normalized with the corresponding classical elasticity results which are summarized below for completeness (Johnson, 1987)

$$a_c = \left(\frac{3PR\,(1-\nu)}{8\mu}\right)^{1/3}, \quad p_{0c} = \left(\frac{24\,P\,\mu^2}{\pi^3\,R^2\,(1-\nu)^2}\right)^{1/3}, \qquad \delta_c = \left(\frac{9\,P^2\,(1-\nu)^2}{64\,R\,\mu^2}\right)^{1/3}. \tag{63}$$

It is observed that the all three ratios present strong dependence upon the ratio ℓ/a and the Poisson's ratio ν . As ℓ/a increases the measured normalized contact

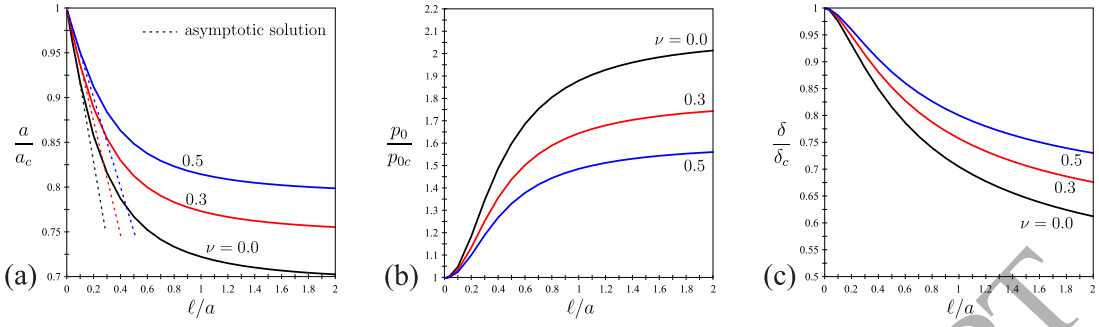

Figure 2: Dependence of the normalized: (a) contact radius a/a_c (b) max pressure p_0/p_{0c} and (c) indentation depth δ/δ_c, upon the ratio ℓ/a and the Poisson's ratio ν. All the results are obtained for a constant applied force P.

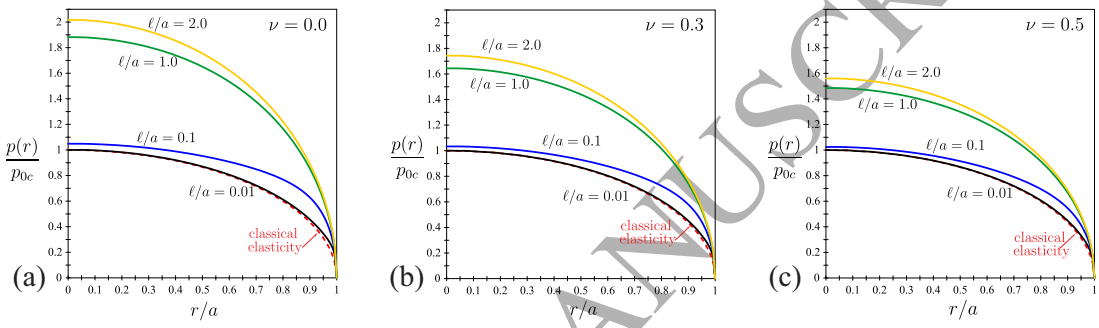

Figure 3: Distribution of the normalized pressure $p(r)/p_{0c}$ below the spherical indenter with respect to the dimensionless radial distance from the center line r/a. The results are presented for selected values of dimensionless microstructural ratio ℓ/a and Poisson's ratio ν. All the results are obtained for a constant applied force P.

radius a/a_c decreases, the normalized maximum normalized pressure p_0/p_{0c} increases, while the normalized indentation depth δ/δ_c decreases suggesting a stiffer response. Regarding the effect of the Poisson's ratio, we note that for increasing ν and fixed value of ℓ/a, the normalized contact radius a/a_c increases, the maximum pressure p_0/p_{0c} decreases and the normalized indentation depth δ/δ_c increases.

It is worth noting that for small values of the microstructural ratio ℓ/a the normalized contact radius in couple-stress elasticity can be given in closed form as:

$$\frac{a}{a_c} = 1 - (1-\nu)\frac{\ell}{a} \qquad \text{for} \quad \ell < 0.2a. \tag{64}$$

The corresponding asymptotic solution is shown in Fig. 2(a) with a dashed line. Substituting a_c from $(63)_1$, we obtain a relation between the applied force P and

the contact radius a in couple-stress elasticity:

$$P = \frac{8\mu\, a^6}{3\,(1-\nu)\,(a-(1-\nu)\,\ell)^3 R}, \qquad \text{(couple-stress elasticity)}, \tag{65}$$

$$P = \frac{8\mu\, a^3}{3\,(1-\nu)\,R}, \qquad \text{(classical Hertz solution)}. \tag{66}$$

The distribution of the contact pressure below the spherical indentor is shown in Figure 3. It is observed that the pressure distribution depends monotonically upon the ratio ℓ/a. For increasing ratios ℓ/a the pressure below the indentor increases significantly. On the other hand, as $\ell/a \to 0$, the classical elliptical pressure distribution is recovered. Furthermore, it is shown that for increasing Poisson's ratio, $p(r)/p_{0c}$ decreases, but $p(r)$ actually increases below the indenter.

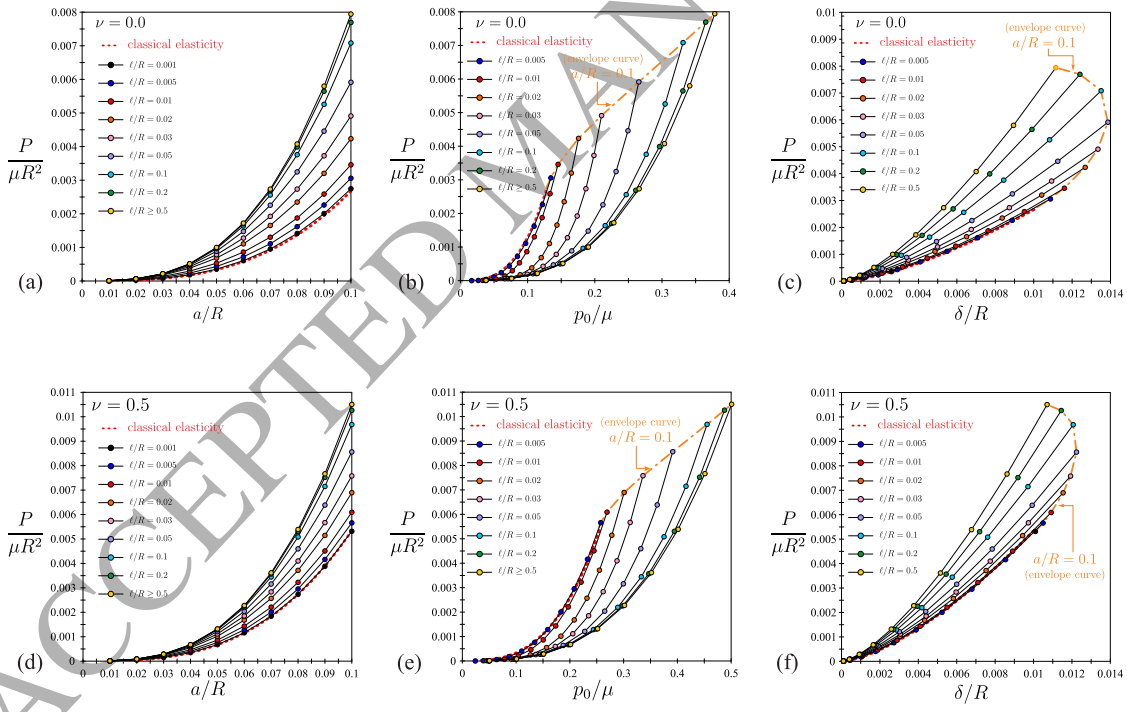

Figure 4: Variation of the normalized load, $P/\mu R^2$ upon the normalized: (a) contact radius, a/R (b) maximum pressure, p_0/μ and (c) indentation depth, δ/R. The results are shown for selected values of the microstructural ratio ℓ/R and Poisson's ratio ν.

Next, in Figure 4 we present the effect of the normalized load, $P/\mu R^2$, upon the normalized: contact radius, a/R (Fig. 4a), maximum pressure, p_0/μ (Fig.

4b), and indentation depth, δ/R (Fig. 4c). The results now are shown for selected values of ℓ/R and two values for the Poisson's ratio: $\nu = 0$ and $\nu = 0.5$. For the results to remain within the frame of the small deformation theory of elasticity, the ratio a/R is kept below the value of 0.1. All curves are bounded therefore by an envelope curve (orange dash-dot line). The corresponding classical elasticity results are also presented (dashed red line). We note that for fixed load P the contact radius a decreases significantly for increasing ℓ/R which shows the stiffening effects predicted by the couple-stress theory. The classical elasticity solution relating $P/\mu R^2$ and a/R is given in equation $(63)_1$. For $\ell/R \simeq 0.01$ the classical elasticity solution is essentially recovered while for $\ell/R \geq 0.5$ no further effect of the microstructural length scale is attained and all the curves coincide (see Fig. 4[a,b,d,e]). Regarding the dependence of the normalized load $P/\mu R^2$ with respect to the normalized maximum pressure p_0/μ, we note that for fixed p_0/μ, $P/\mu R^2$ decreases as the normalized microstructural length ℓ/R increases. Finally, the relation between the normalized load $P/\mu R^2$ and the normalized displacement δ/R is presented in Figs (4)c and (4)f. It is shown that for fixed load P the indentation depth δ decreases significantly for increasing ℓ/R which shows clearly the size-effect predicted by the couple-stress theory.

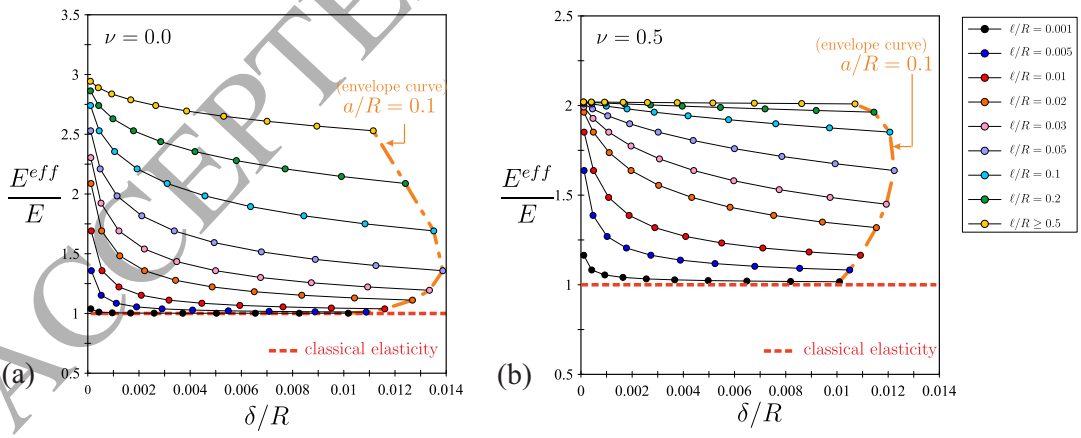

Figure 5: Dependence of the normalized effective Young's modulus of the microstructured material E^{eff}/E upon the normalized indentation depth, δ/R. The results are shown for selected values of dimensionless microstructural ratio ℓ/R and Poisson's ratio ν.

Next, Figure 5 presents the dependence of the normalized effective Young's

modulus of the microstructured material E^{eff}/E upon the normalized indentation depth, δ/R (note that $E = 2\mu(1+\nu)$). Again, results are given for selected values of dimensionless microstructural length ℓ/a and Poisson's ratio ν. The effective Young's modulus can be readily evaluated from equation (63)(a) given the radius R of the indentor, the applied load P, and, in this case, the attained contact radius a (or the indentation depth δ) in the context of couple-stress elasticity. It can be seen that for increasing δ/R the ratio E^{eff}/E decreases while for given δ/R, the ratio E^{eff}/E increases with increasing ℓ/R. Indeed, the attained behavior clearly demonstrates the size effect observed in various experimental studies (see e.g. Alisafaei et al., 2014; Han et al., 2016; Chandrashekar and Han, 2016). To this respect, the experimental results of Alisafaei et al. (2014) illustrate that for epoxy no evident size effect is attained for $\delta/R \geq 0.002$ while in the work of Han et al. (2016) it is experimentally shown that no evident size effect is attained for $\delta/R \geq 0.024$ for PDMS, both using a spherical indenter with $R = 250\mu$m. In comparison, our results from Fig. 5, indicate that in order no size effect to be obtained the microstructural length should be $\ell \approx 0.25\mu$m for epoxy while the microstructural length should be $\ell \approx 0.25 - 2.5\mu$m for PDMS. Furthermore, it is estimated that if smaller indentation depths were pursued in the PDMS indentation experiment, size effects would have probably appeared. This is also supported by further experiments using Berkovich indentors, in which the evaluated effective modulus does not reach a plateau at small indentation depths. Of course, sharp indentors seem to be more sensitive in capturing size effects as has been experimentally shown in the works of Alisafaei et al. (2014) and Han et al. (2016) but also theoretically shown by Zisis et al. (2014). Nevertheless, the spherical indenter may be advantageous in cases where limited or no damage at the surface is in need. Furthermore, from the same set of results it is inferred that for decreasing R the effective Young's modulus E^{eff} increases in accordance with the results of Garg et al. (2016).

In what follows, we present some details regarding the behavior of the surafce

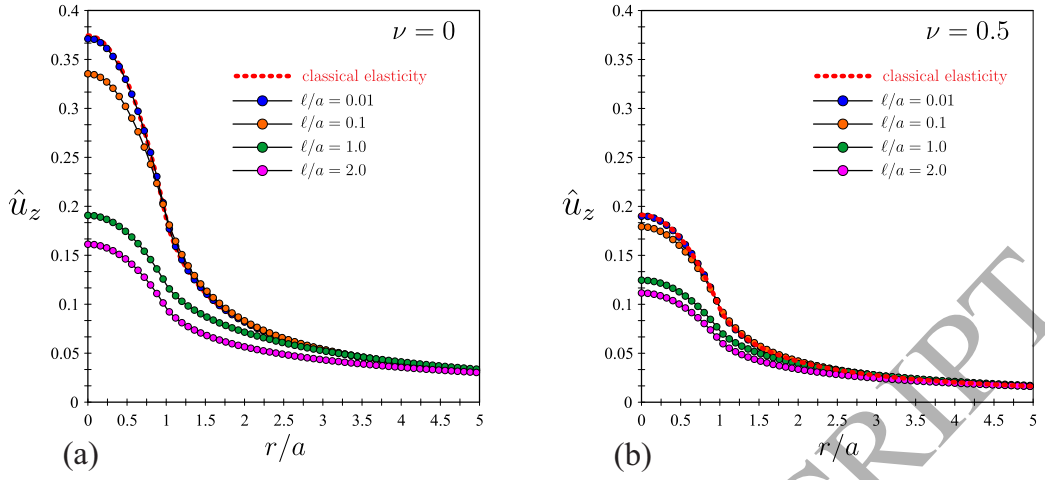

Figure 6: Variation of the normalized vertical displacement $\hat{u}_z$ with respect to the normalized radial distance from the center line r/a. The results are shown for selected values of microstructural ratio ℓ/a and Poisson's ratio ν. All the results are obtained for a constant applied force P.

displacements and selected stress fields. In Figures 6 and 7, we depict the dependence of the normalized vertical displacement $\hat{u}_z = \{a\mu/P)\, u_z(r,0)$ and the normalized radial displacement $\hat{u}_r = (a\mu/P)\, u_r(r,0)$ upon the normalized radial distance from the center line r/a for selected values of microstructural ratios ℓ/a and Poisson's ratios ν. The classical elasticity solutions are plotted over for comparison according to equations (67) and (68) shown below (Johnson, 1987)

for $r \leq a_c$

$$u_z^{cl.}(r) = \frac{(1-\nu)\pi\, p_{0c}\, a_c}{8\mu}\left(2 - \frac{r^2}{a_c^2}\right),$$
$$u_r^{cl.}(r) = -\frac{(1-2\nu)}{6\mu}\frac{p_{0c}\, a_c^2}{r}\left[1 - \left(1 - \frac{r^2}{a_c^2}\right)^{3/2}\right], \tag{67}$$

for $r > a_c$,

$$u_z^{cl.}(r) = \frac{(1-\nu)p_{0c}\, a_c}{4\mu}\left[\left(2 - \frac{r^2}{a_c^2}\right)\, \sin^{-1}\left(\frac{a_c}{r}\right) + \frac{r}{a_c}\left(1 - \frac{a_c^2}{r^2}\right)^{1/2}\right],$$
$$u_r^{cl.}(r) = -\frac{(1-2\nu)}{6\mu}\frac{p_{0c}\, a_c^2}{r}\left[1 - \left(1 - \frac{r^2}{a_c^2}\right)^{3/2}\right], \tag{68}$$

It is observed that for increasing ℓ/a, the vertical displacement $\hat{u}_z$ below the indenter decreases suggesting a stiffer material response, while for distances $r \geq 4a$ from the centre line the couple-stress effects diminish and the curves converge to the classical Hertz solution. Further information is obtained from the behaviour of the normalized radial displacement $\hat{u}_r$ with respect to ℓ/a. In this case, we note that for $\nu = 0$ classical elasticity suggests negative radial displacements along the surface of the half-space while for increasing ℓ/a the radial displacements change sign and become positive throughout $\ell/a \geq 2$. In marked contrast with the classical Hertz solution, the radial displacement in couple-stress elasticity is not zero for an incompressible material ($\nu = 0.5$). On the contrary, as ℓ/a increases $\hat{u}_r$ increases significantly attaining a peak value at the end of the contact region ($r = a$).

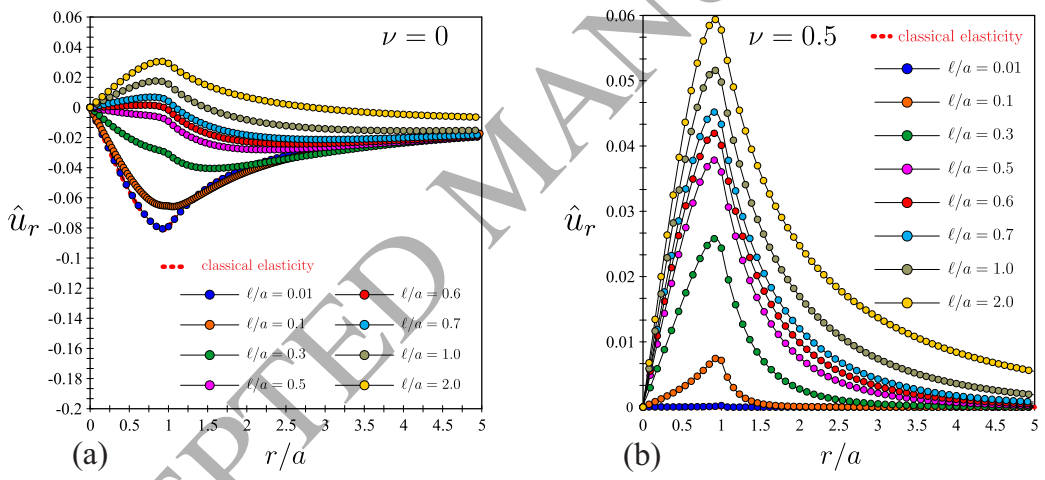

Figure 7: Variation of the normalized radial displacement $\hat{u}_r$ with respect to the normalized radial distance from the center line r/a. The results are shown for selected values of microstructural ratio ℓ/a and Poisson's ratio ν. All the results are obtained for a constant applied force P.

In Figure 8, we present the dependence of the normalized rotation $\hat{\omega}_\theta = \{a^2\mu/P\}\,\omega_\theta(r,0)$ upon the normalized radial distance from the center line r/a for selected values of the microstructural ratio ℓ/a and Poisson's ratio ν. The peak value for the surface rotation is obtained at the end of the contact area ($r = a$). It is observed that for increasing ℓ/a the rotations below and outside the indenter decrease showing that when the microstructure becomes more pro-

nounced the interface between the indenter and the half-plane becomes stiffer. An interesting discussion of interface conditions in couple-stress theory is given by Weitsman (1965). Note that for $r \geq 4a$ the couple-stress effects essentially vanish. Finally, from the same Figure, we can further deduce that the surface rotation $\hat{\omega}_\theta$ increases with increasing R (assuming constant P and ℓ). This effect is less pronounced for higher values of the Poisson's ratio in accord with classical elasticity.

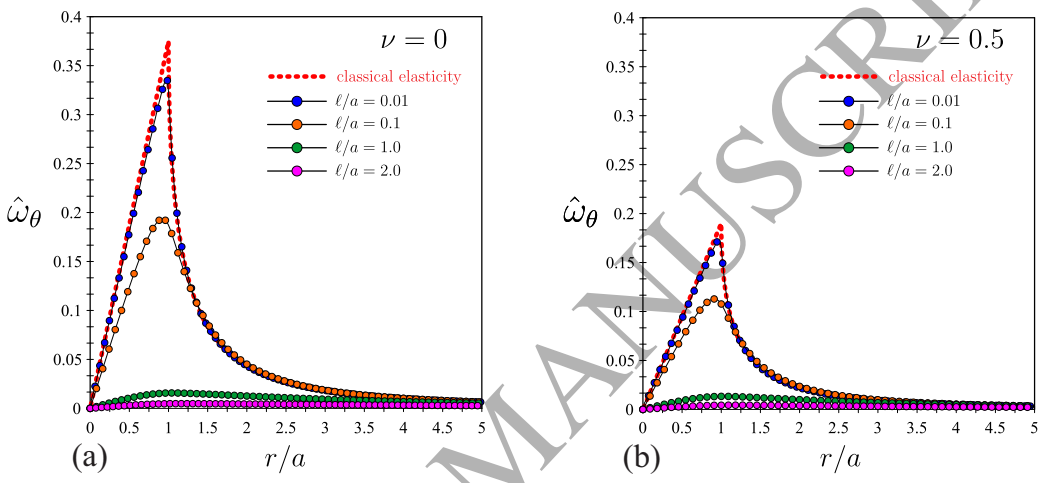

Figure 8: Variation of the normalized rotation $\hat{\omega}_\theta$ upon the normalized radial distance from the center line r/a. The results are shown for selected values of microstructural ratio ℓ/a and Poisson's ratio ν. All the results are obtained for a constant applied force P.

Regarding the stress field in the half-space, it should first be noted that due the axisymmetric nature of the problem, the non-vansishing shear stress components along the center line $r = 0$ are zero, i.e. $\sigma_{zr} = \sigma_{rz} = 0$. Moreover, using Eqs (41) and (42), it can be readily shown that $\sigma_{rr}(r, 0) = \sigma_{\theta\theta}(r, 0)$. The above observations imply that normal stresses $(\sigma_{rr}, \sigma_{\theta\theta}, \sigma_{zz})$ along the center-line $(r = 0)$ are also principal stresses. Therefore, the principal shear stress along the center line is given as: $\tau_{\max} = 0.5|\sigma_{rr} - \sigma_{zz}|$, and it is indeed the maximum shear stress in the field as in classical elasticity. Figure 9, illustrates the variation of $\tau_{\max}$, with respect to the normalized distance z/a. In the classical Hertz solution, the maximum value of the shear stress lies below the surface and exceeds the principal shear stress at the origin. In fact, it has been shown that $\tau_{\max} = 0.384\, p_{0c}$ at $z = 0.38a_c$

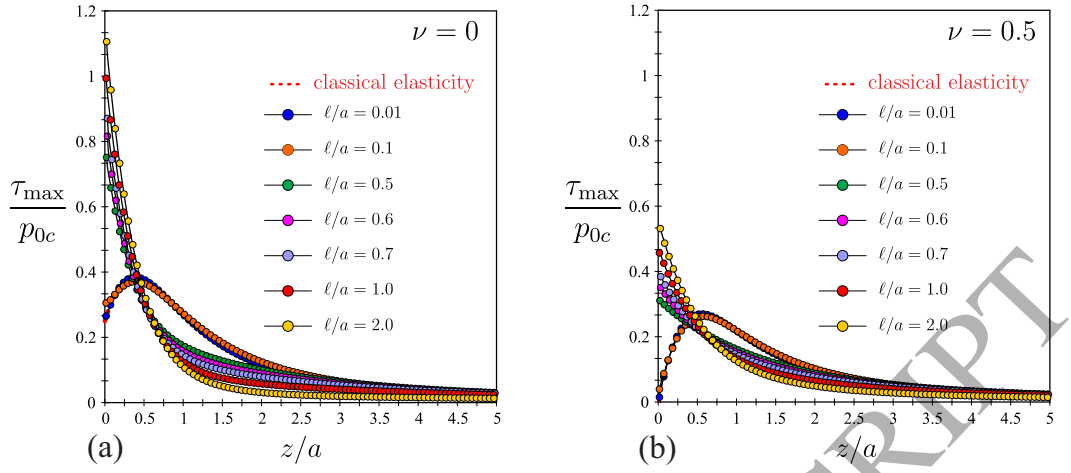

Figure 9: Variation of the normalized max shear stress $\tau_{\max}/p_{0c}$ upon the normalized distance along the center line from the surface z/a. The results are shown for selected values of dimensionless microstructural length ℓ/a and Poisson's ratio ν. All the results are obtained for a constant applied force P.

for $\nu = 0$, and $\tau_{\max} = 0.226\, p_{0c}$ at $z = 0.54a_c$ for $\nu = 0$ (see e.g. Johnson, 1987). In this case the plastic yielding would be expected to initiate beneath the surface. On the other hand, as the microstructural ratio ℓ/a increases (note that as ℓ increases, a always decreases, for constant load P), $\tau_{\max}$ increases significantly, while its maximum value is attained now essentially at the surface. Furthermore, it is noted that for $\ell/a \leq 0.1$, no effect upon the magnitude or the position of $\tau_{\max}$ is observed. For design purposes, to confine yielding near the surface of the material a coarse microstructure is desirable, while a fine microstructure shields the surface from yielding. We note that similar effects have been observed in the indentation of graded materials where the attained stress fields shrink normally to the region of the applied load while they expand laterally for finer microstructural characteristics, see Zisis et al. (2010). Finally, we should mention the work by Gao and Zhou (2013) who presented a solution treated in the context of gradient elasticity. Even though some general qualitative comparison can be drawn, it should be noted that on one hand this work employs a different generalized theory than the couple stress elasticity, while on the other hand the authors solve a pure traction boundary value problem imposing the classical elliptical stress distribution on the surface of the half-space at an a priori known contact area.

Both solutions show stiffening effects evidenced by the decrease of the surface displacements with increasing microstructural length scale and by the decrease of the average pressure with increasing contact area. However, as it can be seen from the present results the elliptical pressure profile obtained in classical elasticity according to the Hertzian solution is significantly altered in the presence of couple stresses. This has also been shown in two dimensional contact problems in the context of couple stress elasticity as shown by Gourgiotis and Zisis (2016) and similar results are expected in the case of gradient elasticity.

6 Conclusions

Significant size-effects, which are the result of the existence of material characteristic lengths, have been observed during indentation of microstructured materials. To this respect we studied the spherical indentation technique in the context of couple stress elasticity, which is a simple yet very effective generalized continuum theory for modeling microstructured materials. Our purpose was to examine to what extend this rather simple gradient-type theory captures the experimentally observed indentation response including the reported size effects. The present study suggests an extension of the classical Hertz contact problem and we believe that will give useful theoretical guidance for the interpretation of spherical indentation tests of microstructured materials. In fact, the results show significant departure from the well-known classical elasticity predictions, as suggested by Hertz and other researchers. It was shown that as the microstructural length becomes more pronounced, the pressure below the indenter increases, while both the contact radius and the indentation depth decrease compared to the classical elasticity predictions, suggesting thus a stiffer response. A simple closed form relation between the applied load P and the resulting contact area a is proposed that takes into account the material microstructure through the characteristic length ℓ. In comparison to available experimental results, our solution indicates

that the microstructural length of epoxy and DPMS is approximately equal to $\ell \approx 0.25\mu$m and $\ell \approx 0.25 - 2.5\mu$m, respectively. Furthermore, details regarding the attained stress fields are reported and compared to the corresponding classical elasticity results. It is finally shown that the principal shear stress attains its maximum at surface in contrast to the classical elasticity where the maximum principal shear stress lies below the surface. Hence plastic yielding is expected to initiate at confined regions adjacent to the surface.

References

Alisafaei, F., Han, C.-S., and Lakhera, N. Characterization of indentation size effects in epoxy. Polymer Test., 40:70–78, 2014.

Alisafaei, F., Han, C.-S., and Sanei, S.H.R. On the time and indentation depth dependence of hardness, dissipation and stiffness in polydimethylsiloxane. Polymer Test., 32(7):1220–1228, 2013.

Anagnostou, D.S., Gourgiotis, P.A. and Georgiadis, H.G. The Cerruti problem in dipolar gradient elasticity. Mathematics and Mechanics of Solids, 20(9), 1088-1106, 2015.

Bigoni, D. and Gourgiotis, P.A. Folding and faulting of an elastic continuum. Proc. R. Soc. Lond. A, 472(2187):20160018, 2016.

Briscoe, B.J., Fiori, L., and Pelillo, E. Nano-indentation of polymeric surfaces. J. Phys. D, 31(19):2395, 1998.

Cao, Y., Allameh, S., Nankivil, D., Sethiaraj, S., Otiti, T., and Soboyejo, W. Nanoindentation measurements of the mechanical properties of polycrystalline Au and Ag thin films on silicon substrates: Effects of grain size and film thickness. Mater. Sci. Eng. A, 427(1-2):232–240, 2006.

Chandrashekar, G. and Han, C.S. Length scale effects in epoxy: The dependence of elastic moduli measurements on spherical indenter tip radius. Polymer Testing 53, 227-233, 2016.

Chong, A.C.M. and Lam, D.C.C. Strain gradient plasticity effect in indentation hardness of polymers. J. Mater. Res., 14(10):4103–4110, 1999.

Civelek, M.B. and Erdogan, F. The axisymmetric double contact problem for a frictionless elastic layer. Int. J. Solids Struct., 10(6):639–659, 1974.

Dutta, A.K., Penumadu, D., and Files, B. Nanoindentation testing for evaluating modulus and hardness of single-walled carbon nanotube–reinforced epoxy composites. J. Mater. Res., 19(1):158–164, 2004.

Ejike, U.B.C.O. The plane circular crack problem in the linearized couplestress theory. Int. J. Eng. Sci., 7(9):947–961, 1969.

Ejike, U.B.C.O. Boundary effects due to body forces and body couples in the interior of a semi-infinite elastic solid. International Journal of Engineering Science, 8(11), 909-924, 1970.

Erdogan, F. Stress distribution in bonded dissimilar materials containing circular or ring-shaped cavities. J. Appl. Mech., 32(4):829–836, 1965.

Flores, A. and Baltá Calleja, F.J. Mechanical properties of poly(ethylene terephthalate) at the near surface from depth-sensing experiments. Philos. Mag. A, 78(6):1283–1297, 1998.

Gao, X.L. and Zhou, S.S. Strain gradient solutions of half-space and half-plane contact problems. Zeitschrift für angewandte Mathematik und Physik, 64(4), 1363-1386, 2013.

Garg, N. Han, C.S. and Alisafaei, F. Length scale dependence in elastomers-Comparison of indentation experiments with numerical simulations. Polymer 98, 201-209, 2016.

Georgiadis, H.G., Gourgiotis, P.A., Anagnostou, D.S. The Boussinesq problem in dipolar gradient elasticity. Archive of Applied Mechanics 84, 1373-1391, 2014.

Giannakopoulos, A.E. and Parmaklis, A.Z. The contact problem of a circular rigid punch on piezomagnetic materials. Int. J. Solids Struct., 44(14-15):4593–4612, 2007. Giannakopoulos, A.E. and Suresh, S. Theory of indentation of piezoelectric materials. Acta Mater., 47(7):2153–2164, 1999.

Gourgiotis, P.A. and Bigoni, D. Stress channelling in extreme couple-stress materials part I: Strong ellipticity, wave propagation, ellipticity, and discontinuity relations. J. Mech. Phys. Solids, 88:150–168, 2016.

Gourgiotis, P.A. and Georgiadis, H.G. An approach based on distributed dislocations and disclinations for crack problems in couple-stress elasticity. Int. J. Solids Struct., 45:5521–5539, 2008.

Gourgiotis, P.A. and Georgiadis, H.G. Distributed dislocation approach for cracks in couple-stress elasticity: shear modes. Int. J. Fract., 147:83–102, 2007.

Gourgiotis, P. and Zisis, T. Two-dimensional indentation of microstructured solids characterized by couple-stress elasticity. The Journal of Strain Analysis for Engineering Design, 51(4), 318-331, 2016.

Gourgiotis, P.A., Zisis, Th., and Baxevanakis, K.P. Analysis of the tilted flat punch in couple-stress elasticity. Int. J. Solids Struct., 85:34–43, 2016.

Han, C.-S. Influence of the molecular structure on indentation size effect in polymers. Mater. Sci. Eng. A, 527(3):619–624, 2010.

Han, C.-S., Sanei, S.H.R., and Alisafaei, F. On the origin of indentation size effects and depth dependent mechanical properties of elastic polymers. J. Polym. Eng., 36(1):103–111, 2016.

Hertz, H. On the contact of elastic solids. Journal für die Reine und Angewandte Mathematik, 92:156–171, 1881.

Hills, D.A., Kelly, P., Dai, D., Korsunsky, A., 1996. Solution of crack problems: the distributed dislocation technique. Springer Science and Business Media.

Johnson, K.L., Kendall, K., and Roberts, A.D. Surface energy and the contact of elastic solids. Proc. R. Soc. Lond. A, 324(1558):301–313, 1971.

Johnson, K.L. Contact mechanics. Cambridge University Press, 1987.

Karuriya, A.N. and Bhandakkar ,T.K. Plane strain indentation on finite thickness bonded layer in couple stress elasticity. Int. J. Solids Struct., 108:275– 288, 2017.

Koiter .W.T. Couple stresses in the theory of elasticity, I and II. Proc. K. Ned. Akad. Wet. (B), 67:17–44, 1964.

Lam, D.C.C. and Chong, A.C.M. Indentation model and strain gradient plasticity law for glassy polymers. J. Mater. Res., 14(9):3784–3788, 1999.

Lam, D.C.C. and Chong, A.C.M. Effect of cross-link density on strain gradient plasticity in epoxy. Mater. Sci. Eng. A, 281(1-2):156–161, 2000.

Lam, D.C.C. and Chong, A.C.M. Characterization and modeling of specific strain gradient modulus of epoxy. J. Mater. Res., 16(2):558–563, 2001.

Lim, Y.Y. and Chaudhri, M.M. Indentation of elastic solids with a rigid Vickers pyramidal indenter. Mech. Mater., 38(12):1213–1228, 2006.

McFarland, A.W. and Colton, J.S. Role of material microstructure in plate stiffness with relevance to microcantilever sensors. J. Micromech. Microeng., 15(5):1060, 2005.

Mao, S., Purohit, P.K., and Aravas, N. Mixed finite-element formulations in piezoelectricity and flexoelectricity. Proc. R. Soc. A, 472(2190):20150879, 2016.

Morini, L., Piccolroaz, A., Mishuris, G., and Radi, E. On fracture criteria for dynamic crack propagation in elastic materials with couple stresses. Int. J. Eng. Sci., 71:45–61, 2013.

Mindlin, R.D. and Tiersten, H.F. Effects of couple-stresses in linear elasticity. Arch. Ration. Mech. Anal., 11:415–448, 1962.

Mishuris, G., Piccolroaz, A., and Radi, E. Steady-state propagation of a mode III crack in couple stress elastic materials. Int. J. Eng. Sci., 61:112–128, 2012.

Muki, R. and Sternberg, E. The influence of couple-stresses on singular stress concentrations in elastic solids. ZAMP, 16:611–648, 1965.

Nikolov, S., Han, C.-S., and Raabe, D. On the origin of size effects in smallstrain elasticity of solid polymers. Int. J. Solids Struct., 44(5):1582–1592, 2007.

Nix, W.D. and Gao, H. Indentation size effects in crystalline materials: a law for strain gradient plasticity. J. Mech. Phys. Solids, 46(3):411–425, 1998.

Radi, E. On the effects of characteristic lengths in bending and torsion on mode III crack in couple stress elasticity. Int. J. Solids Struct., 45:3033–3058, 2008.

Shen, L., Liu, T., and Lv, P. Polishing effect on nanoindentation behavior of nylon 66 and its nanocomposites. Polymer Test., 24(6):746–749, 2005.

Shu, J.Y. and Fleck, N.A. The prediction of a size effect in microindentation. Int. J. Solids Struct., 35(13):1363 – 1383, 1998.

Song, H.X., Ke, L.L., and Wang, Y.S. Sliding frictional contact analysis of an elastic solid with couple stresses. Int. J. Mech. Sci., 133:804–816, 2017.

Swaddiwudhipong, S., Poh, L.H., Hua, J., Liu, Z.S., and Tho, K.K. Modeling nano-indentation tests of glassy polymers using finite elements with strain gradient plasticity. Mater. Sci. Eng. A, 404(1-2):179–187, 2005.

Voyiadjis, G.Z., Shojaei, A., and Mozaffari, N. Strain gradient plasticity for amorphous and crystalline polymers with application to micro-and nano-scale deformation analysis. Polymer, 55(16):4182–4198, 2014.

Weitsman, Y. Couple-stress effects on stress concentration around a cylindrical inclusion in a field of uniaxial tension. ASME J. Appl. Mech., 32(2):424–428, 1965.

Zhang, T.-Y., Xu, W.-H., and Zhao, M.-H. The role of plastic deformation of rough surfaces in the size-dependent hardness. Acta Mater., 52(1):57–68, 2004.

Zhang, T.-Y. and Xu, W.-H. Surface effects on nanoindentation. J. Mater. Res., 17(7):1715–1720, 2002.

Zisis, Th. Anti-plane loading of microstructured materials in the context of couple stress theory of elasticity: half-planes and layers. Arch. Appl. Mech., pages 1–14, 2017.

Zisis, Th., Gourgiotis, P.A., Baxevanakis, K.P., and Georgiadis, H.G. Some basic contact problems in couple stress elasticity. Int. J. Solids Struct., 51:2084– 2095, 2014.

Zisis, Th., Gourgiotis, P.A., and Dal Corso, F. A contact problem in couple stress thermoelasticity: the indentation by a hot flat punch. Int. J. Solids Struct., 63:226–239, 2015.

Zisis, Th., Kordolemis, A., and Giannakopoulos, A.E. Development of strong surfaces using functionally graded composites inspired by natural teeth-finite element and experimental verification. J. Eng. Mater. Technol., 132(1):011010, 2010.